How to cite: *Angew. Chem. Int. Ed.* **2021**, *60*, 24534–24542
International Edition: doi.org/10.1002/anie.202107223
German Edition: doi.org/10.1002/ange.202107223

Analytical Methods Hot Paper

High-Throughput Single-Cell Mass Spectrometry Reveals Abnormal Lipid Metabolism in Pancreatic Ductal Adenocarcinoma

*Qinlei Liu[+], Wenjie Ge[+], Tongtong Wang, Jiayi Lan, Sandra Martínez-Jarquín, Christian Wolfrum, Markus Stoffel, and Renato Zenobi**

Abstract: *Even populations of clonal cells are heterogeneous, which requires high-throughput analysis methods with single-cell sensitivity. Here, we propose a rapid, label-free single-cell analytical method based on active capillary dielectric barrier discharge ionization mass spectrometry, which can analyze multiple metabolites in single cells at a rate of 38 cells/minute. Multiple cell types (HEK-293T, PANC-1, CFPAC-1, H6c7, HeLa and iBAs) were discriminated successfully. We found evidence for abnormal lipid metabolism in pancreatic cancer cells. We also analyzed gene expression in a cancer genome atlas dataset and found that the mRNA level of a critical enzyme of lipid synthesis (ATP citrate lyase, ACLY) was upregulated in human pancreatic ductal adenocarcinoma (PDAC). Moreover, both an ACLY chemical inhibitor and a siRNA approach targeting ACLY could suppress the viability of PDAC cells. A significant reduction in lipid content in treated cells indicates that ACLY could be a potential target for treating pancreatic cancer.*

Introduction

There are differences between individual cells, and even in the same cell population, cell heterogeneity exists.[1] Among the reasons are genetic differences and stochastic processes that occur in the cellular metabolism.[2] Since population measurements conceals information about the heterogeneity between cells, it is important to have sensitive analytical methods that afford the accurate chemical composition and contents of single cells. In addition, rare cell types including circulating tumor cells, cancer stem cells, invariant natural killer T cells, antigen-specific T cells, etc., play significant roles in pathogenic mechanisms, early diagnosis of tumor, and angiogenesis in cancer and other diseases.[3] In order to understand the results of these genetic differences and stochastic processes in individual cells more deeply and faithfully reflect the role that cells play in the regular operation of biological systems in terms of structure and function, it is necessary to analyze and study the composition and chemical content of cells at the single-cell level.

The concept of single-cell analysis has received widespread attention in recent years and has important applications.[4] Various single-cell omics technologies have emerged, including single-cell genomics, transcriptomics, proteomics and metabolomics. Also, Single-cell omics technologies have been applied to reveal metabolic heterogeneity of cells.[5] Compared to single-cell genomics, transcriptomics, and proteomics, single-cell metabolomics provides more rapid and dynamic information of cell function. For example, a deregulated metabolism is a hallmark of cancer cells.[6] Specifically, a dramatic increase of the de novo biosynthesis of fatty acids is generally observed in tumor cells. The increased capacity for generating lipids not only facilitates the formation of lipid bilayers but also enables the tumor cells to modulate their specific signaling transduction and cope with oxidative stress.[7] For example, pancreatic ductal adenocarcinoma (PDAC) is one of the most lethal cancers with only around 9% 5-year survival rate.[8] Accumulation of fatty acids was reported to correlate with PDAC initiation and metastasis in a PDAC mouse model,[9] indicating that lipid metabolism may be dysregulated in PDAC. Cancer cells are highly heterogeneous and exhibit phenotypic diversity, and the heterogeneity of cancer is closely related to the pathogenesis of cancer.[10] Single-cell analysis can accurately characterize the heterogeneity of cancer, thereby providing cancer treatment strategies.[11]

Single-cell analysis is challenging because intracellular biochemical reaction rates are fast, intracellular composition is very complex, the sample size is very small, some compounds are present only at the trace level, may have poor stability, and may be structurally similar. Studying the biological properties of single cells requires analytical techniques with high sensitivity, the ability to analyze ultra-small samples, good selectivity, and fast response. Since mass spectrometry has high sensitivity and selectivity, it holds great promise as an effective technique for single-cell metabolomics analysis. Numerous mass spectrometric techniques have

[*] Q. Liu,[+] J. Lan, Dr. S. Martínez-Jarquín, Prof. Dr. R. Zenobi
Department of Chemistry and Applied Biosciences, ETH Zurich
Vladimir-Prelog-Weg 3, 8093 Zurich (Switzerland)
E-mail: zenobi@org.chem.ethz.ch
Dr. W. Ge,[+] Prof. Dr. M. Stoffel
Department of Biology, ETH Zurich
Otto-Stern-Weg 7, 8093 Zurich (Switzerland)
T. Wang, Prof. Dr. C. Wolfrum
Department of Health Sciences and Technology, ETH Zurich
Schorenstrasse 16, 8603 Schwerzenbach (Switzerland)
[+] These authors contributed equally to this work.
Supporting information and the ORCID identification number(s) for the author(s) of this article can be found under: https://doi.org/10.1002/anie.202107223.

been developed to elucidate the molecular profiles at the cellular level, including secondary ion mass spectrometry (SIMS),[12] matrix-assisted laser desorption/ionization mass spectrometry (MALDI-MS)[13] and electrospray ionization mass spectrometry (ESI-MS).[14] There are many ESI-based single-cell analytical methods, such as laser ablation-ESI-MS,[15] single probe ESI,[14c] and T-probe ESI,[16] capillary electrophoresis-ESI-MS[17] and so on, however, most of them are low-throughput. Mass Cytometry (CyTOF) is a powerful plasma-based single-cell analysis tool that combines inductively coupled plasma mass spectrometry and flow cytometry.[18] CyTOF can simultaneously detect multiple cell surface protein markers at the single-cell level, but does not detect low molecular weight metabolites. Recently, ESI-MS has been used as a flow cytometry detector to achieve high-throughput analysis of single-cell metabolites.[19] To widen the metabolome coverage, alternative ionization methods are useful.

Here we therefore explore the use of dielectric barrier discharge ionization (DBDI) for single-cell metabolomics. DBDI operates without auxiliary reagents and at atmospheric pressure, is easy to miniaturize, easy to operate, cheap and efficient, and has been used for the ionization of small molecular weight metabolites in recent years.[20] The DBDI-MS method introduced here has similar performance in terms of throughput, sensitivity, and the ability to distinguish cell types than the recently reported CyESI-MS methodology.[19] However, compared to other ionization methods, DBDI has some unique properties, for example, it is less affected by matrix effects and ion suppression than ESI,[21] it can analyze polar and nonpolar compounds simultaneously, and does not need vacuum condition.[20a,22] Very recently, we have applied an ESI—DBDI combination source to single plant cell analysis (data not shown here).[23] Compared to ESI, a 2-fold increase in the number of visible metabolites was observed in the combination source.

In this work, we propose a high-throughput and label-free single-cell analytical method based on an active capillary DBDI source,[24] where the ionization takes place inside a capillary that is directly connected to the MS inlet. This dramatically increases robustness and ion transmission into the MS. The DBDI-MS platform (Figure 1) used in this work can analyze multiple metabolites in a single cell at the same time, including organic acids, carbonyl compounds, heterocyclic organic compounds and lipids, and can detect around 38 cells per minute. The proposed DBDI-MS platform was able to discriminate multiple cell types (293T, PANC-1, CFPAC-1, HeLa and iBAs) based on their metabolic profile. Moreover, the abnormal lipid metabolism in pancreatic cancer cells was observed by using the DBDI-MS platform. As one of the major components involved in fatty acyl chain biosynthesis, the enzyme ATP citrate lyase (ACLY) is frequently upregulated in tumor cells.[25] Recently, it has been shown that ACLY is critical for the initiation of PDAC in pancreatic cancer animal model, as ACLY ablation attenuated the acinar-to-ductal metaplasia (ADM).[26] However, the expression levels and potential role of ACLY were not fully elucidated in established PDAC. Here, we propose that the expression levels of ACLY are related to the abnormal lipid metabolism in established PDAC. The DBDI-MS platform specifically detected the redistribution of lipids in PDAC cells after treating them with different dosages of specific ACLY inhibitor but not in PDAC cells treated with a canonical anticancer drug (gemcitabine) or DMSO. Furthermore, both specific chemical inhibitor or siRNA approach targeting ACLY could reduce the cell viability in PDAC cells, indicating the tumor-promoting effect of ACLY in established PDAC cells.

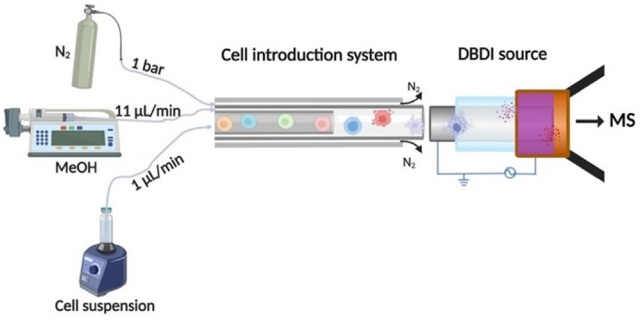

Figure 1. Schematic of the the DBDI-MS platform. Cells are lysed by MeOH in the cell introduction system, and the metabolites in the cells are ionized by DBDI source.

Results and Discussion

Feasibility of Single-Cell DBDI-MS

The specific configuration and operation details of DBDI-MS are shown in Figure S1 and described in full detail in section 1 of the supporting information (SI). Since DBDI-MS has not previously been used for single-cell analysis, we conducted preliminary experiments to demonstrate its feasibility. A PANC-1 cell suspension (at a flow rate of 1 µL min^{-1}) and MeOH (at a flow rate of 11 µL min^{-1}) were introduced into the DBDI source via a home-built cell introduction system (Figure S1). As presented in Figure 2a, signal pulses appeared in the total ion chromatogram (TIC) when the DBDI source was on, but when it was off, even if the cell suspension was introduced into the DBDI source, there was no signal in the TIC. In order to demonstrate that the detected signals came from cells rather than from other substances, the peaks at m/z 760.5851 (assigned to glycerophosphocholine (PC) 34:1) and m/z 732.5538 (assigned to PC 32:1), which are components of cell membranes, were chosen as markers of cells passing through the DBDI. It can be seen from Figure 2b and c that the positions and frequency of m/z 760.5851 and m/z 732.5538 peaks matched with the TIC. Figures 1d, e and f display that with the DBDI switched on, there were obvious lipid peaks in the m/z 700-m/z 900 region, but there were no lipid peaks when the DBDI was turned off. The results suggest that DBDI-MS is able to detect single cells.

The optimization of experimental conditions for single-cell analysis is described in detail in section 2 of the SI (Figure S2–S6). To further evaluate the performance of DBDI-MS, analysis of different cell suspensions was carried

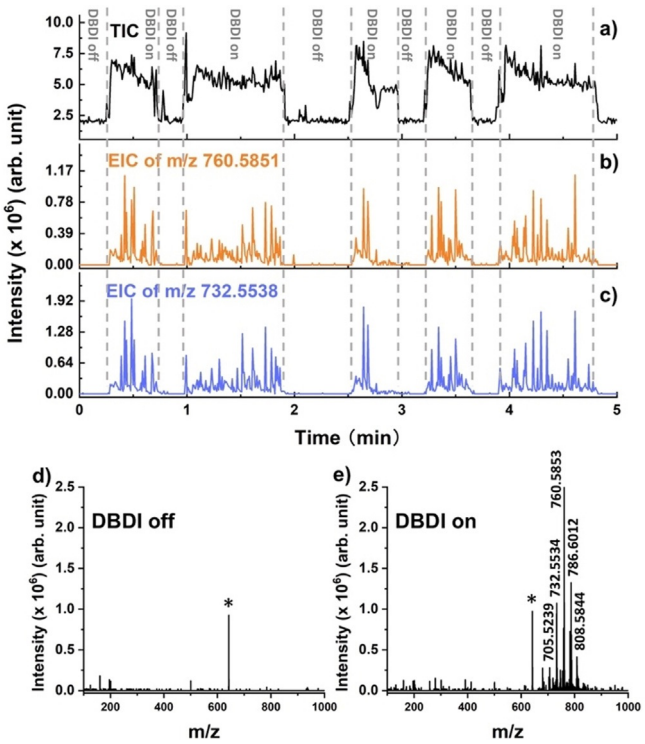

Figure 2. PANC-1 cell analyzed by DBDI-MS. a) Total ion chromatogram (TIC), b) extracted ion chromatogram (EIC) of *m/z* 760.5851 and c) EIC of *m/z* 732.5538 acquired in DBDI on and off modes. d) mass spectrum in DBDI off mode, and e) mass spectrum in DBDI on mode. The asterisk (*) indicates electronic noise in the spectra.

out (in section 3 of the SI, Figure S7–S9), including PANC-1 cells, CFPAC-1 and H6c7 cells. In order to further prove that the results obtained were from single cells instead of cell clusters, the cell suspension was sequentially diluted with ammonium formate to 5×10^3, 1×10^4, 2×10^4, 3×10^4, 4×10^4, 5×10^4 cells mL^{-1} and then measured by DBDI-MS. To facilitate the calculation of cell concentration, the flow rate of the cell suspension during the entire experiment was set to 1 μL min^{-1}. The results are summarized in Video S1, Table 1, Table S1 and Table S2. As shown in Video S1, when the concentration was 4×10^4 cells mL^{-1}, around 20 cells were observed to pass through the capillary in around half a minute. As shown in Table 1, Table S1 and Table S2, the number of peaks per minute matched well with the cell concentration, and the number of detected cells were essentially the same as the calculated number of cell, which indicates that most cells were monodisperse and detected separately. However, when the cell concentration was $\geq5\times10^4$ cells mL^{-1}, we found that there were overlaps between the pulsed signals, and even the capillary used to introduce the cells was sometimes blocked. Therefore, the cell concentration used during the entire experiment was controlled to $<5\times10^4$ cells mL^{-1}. The above results prove that our method is high-throughput and able to detect metabolites with single-cell resolution.

Table 1: Comparison between the calculated and the detected number of PANC-1 cells at different densities of the cell suspension.

Cell density, cell mL^{-1}	Calculated cell number [min]	Detected cell number [min]					Average detected cell number [min]
5×10^3	5	3	6	6	4	4	4.6
1×10^4	10	8	8	9	9	11	9
2×10^4	20	19	23	19	18	17	19.2
3×10^4	30	29	30	26	27	24	27.2
4×10^4	40	39	37	38	36	38	37.6

Metabolite Profiling and Discrimination of Cell Type

In positive ion mode, approximately 179 peaks indicating metabolites in the *m/z* range between 100–1000 were detect in PANC-1 cells (Table S3). These metabolites can be classified as organic acids, carbonyl compounds, heterocyclic organic compounds and lipids.

The details of the detected metabolite classification are shown in Table S4. Because there is only limited cell lysis during the brief contact with the MeOH flow (see Figure S1), the extracted metabolites originate mainly from the cell membranes, i.e., most of them are lipids. Since there are lots of reactive species in the plasma, different product ions were generated. In addition to common product ions such as $[M+H]^+$, $[M+Na]^+$, there were also $[M+H-H_2O]^+$, $[M+H-2H_2O]^+$ and $[M+NH_4]^+$ produced. The tandem MS information can be found in Figure S10.

Cell metabolites are potential biomarkers to distinguish cells. To test if our DBDI-MS could be applied to profile cell types, we measured five different kinds of cells, 293T, PANC-1, CFPAC-1, HeLa and iBAs by DBDI-MS. After obtaining metabolic information, principal component analysis (PCA) (Figure 3a) and t-distributed stochastic neighbor embedding (t-SNE) (Figure S11) were used to separate cell types, which showed that single-cell metabolite information could successfully distinguish cell types. The specific details of the analysis for the metabolic profiles are described in section 1 of the SI. The heat map (Figure 3b) shows the relative intensities of metabolite ions from each cell. This information indicates that the types of single-cell metabolite profiles between different cells are significantly different, and single-cell metabolic information is adequate for cell discrimination.

All the above results showed that the DBDI-MS platform is sensitive, accurate and specific to detect a variety of metabolites.

Single-Cell DBDI-MS Metabolic Profile Identify Deregulated Lipid Metabolism in PDAC Cells

Lipid metabolism is critical for cancer development, but the study on the level of lipid metabolism in PDAC cells is still very limited. Thus, we compared the metabolites of PDAC cells and ductal epithelial cells H6c7. By comparing the mass spectral profiles of PANC-1, CFPAC-1 and H6c7 (Figure 4a, b and c), we found that most of the detected compounds are phospholipids. Phospholipids are the main components of cell membranes, and their content in cells is high. In the lower mass range ($m/z<400$), PANC-1 and CFPAC-1 contained hexanoylcarnitine, which was not detectable in H6c7. In the

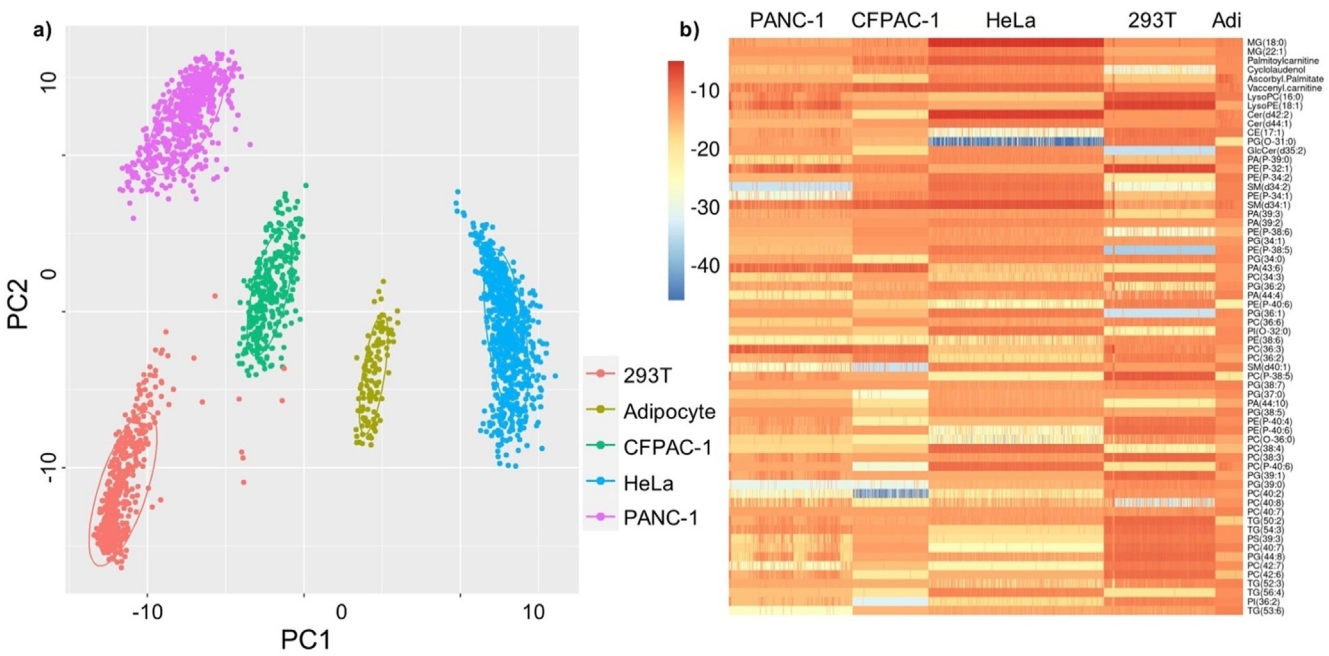

Figure 3. Discrimination of cells by the DBDI-MS platform. a) Principal component analysis (PCA) of five cell types. b) Heatmap of the single-cell metabolite in five cell types.

higher mass range ($m/z > 400$), the most abundant lipids in PANC-1, CFPAC-1 and H6c7 were PC(32:1), PC(34:1), PC(36:2) and PC(38:5), but their distribution was slightly different. As shown in Figure 4a, b, c and S12, in PANC-1 and CFPAC-1, PC (34:1) is the most abundant lipid, its intensity at m/z 760.58 being higher than that of PC (36:2) (m/z 786.60). However, in H6c7, PC (36:2) is the most abundant lipid, with an intensity of PC (34:1) (m/z 760.58) lower than that of PC (36:2) (m/z 786.60). As shown in Figure 4d, e, f and g, the content of PC(32:1), PC(34:1), PC(36:2) and PC(38:5) is higher in pancreatic cancer cell types (PANC-1 and CFPAC-1) than that in pancreatic ductal epithelial cells (H6c7). In addition to these lipids that occur in all three types, each of the cell also contained some unique lipids. For example, PC (O-36:1) and PS (40:3) were only detected in CFPAC-1, and TG (48:2) was only detected in H6c7.

The heat map in Figure S13 shows the normalized intensities of assigned metabolites from each cell, and significant differences are seen for some metabolites. In the volcano plots, differentially expressed features in the two pancreatic cancer cell lines (PANC-1, CFPAC-1) and the corresponding normal cell line (H6c7) are visualized. According to Figure 4h, several amino acids and lipids, for example, *N*-lactoyl-methionine (m/z 239.1061, $[M+NH_4]^+$), hexanoylcarnitine (m/z 260.1856, $[M+H]^+$), MG(18:0) (m/z 381.2981, $[M+Na]^+$) and PS(30:2) (m/z 686.4395, $[M+H-H_2O]^+$) exhibited clear statistical differences between PANC-1 and H6c7 cells. As shown in Figure 4i, the metabolites with statistical differences between CFPAC-1 and H6c7 cells were also amino acids and lipids, for example, PC (34:1) (m/z 782.5660, $[M+Na]^+$), *N*-lactoyl-methionine (m/z 239.1061, $[M+NH_4]^+$) and hexanoylcarnitine (m/z 260.1856, $[M+H]^+$).

To further estimate the potential of DBDI-MS in clinical applications, we carried out an analysis of a mixed cell suspension composed of PANC-1, CFPAC-1 and H6c7 cells, to simulate potentially cancerous tissues of PDAC patients. Based on their characteristic single-cell metabolite profiles acquired by DBDI-MS, DBDI-MS can specifically and high-throughput identify different cell types in a cell mixture (Figure 4j). PANC-1 cells, CFPAC-1 cells, H6c7 cells and the cell mixture can be separated by t-SNE (Figure 4k), and cells from the mixture each fall into a specific group, which makes it possible to blindly identify cells from a mixture.

It can be seen that the types, content and distribution of lipids in pancreatic cancer cells and normal ductal cells are different, and that the abnormal lipid metabolism in pancreatic cancer cells can be clearly observed by DBDI-MS.

Deregulated ACLY Levels in PDAC

In order to investigate why lipid metabolism was abnormal in PDAC cells, we monitored the expression levels of ACLY which is the critical rate-limiting enzyme for lipid synthesis, in one human TCGA dataset consists of 167 normal and 179 PDAC patients.[27] The mRNA level of ACLY increased around 1.4 fold in PDAC (Figure 5a). We further confirmed the upregulated ACLY mRNA levels in PDAC cells by qPCR (Figure 5b). Since ACLY is one of the critical enzymes for acetyl-CoA and lipid acids synthesis, we also analyzed the acetyl-CoA and lipid metabolism biological pathways in the same TCGA dataset by Gene set Enrichment Analysis (GSEA). Interestingly, we found that the genes involved in the acetyl-CoA metabolic process and lipid homeostasis were enriched in human PDAC samples (Figures S14a and b). Combined with our in vitro data (Figure 4), we

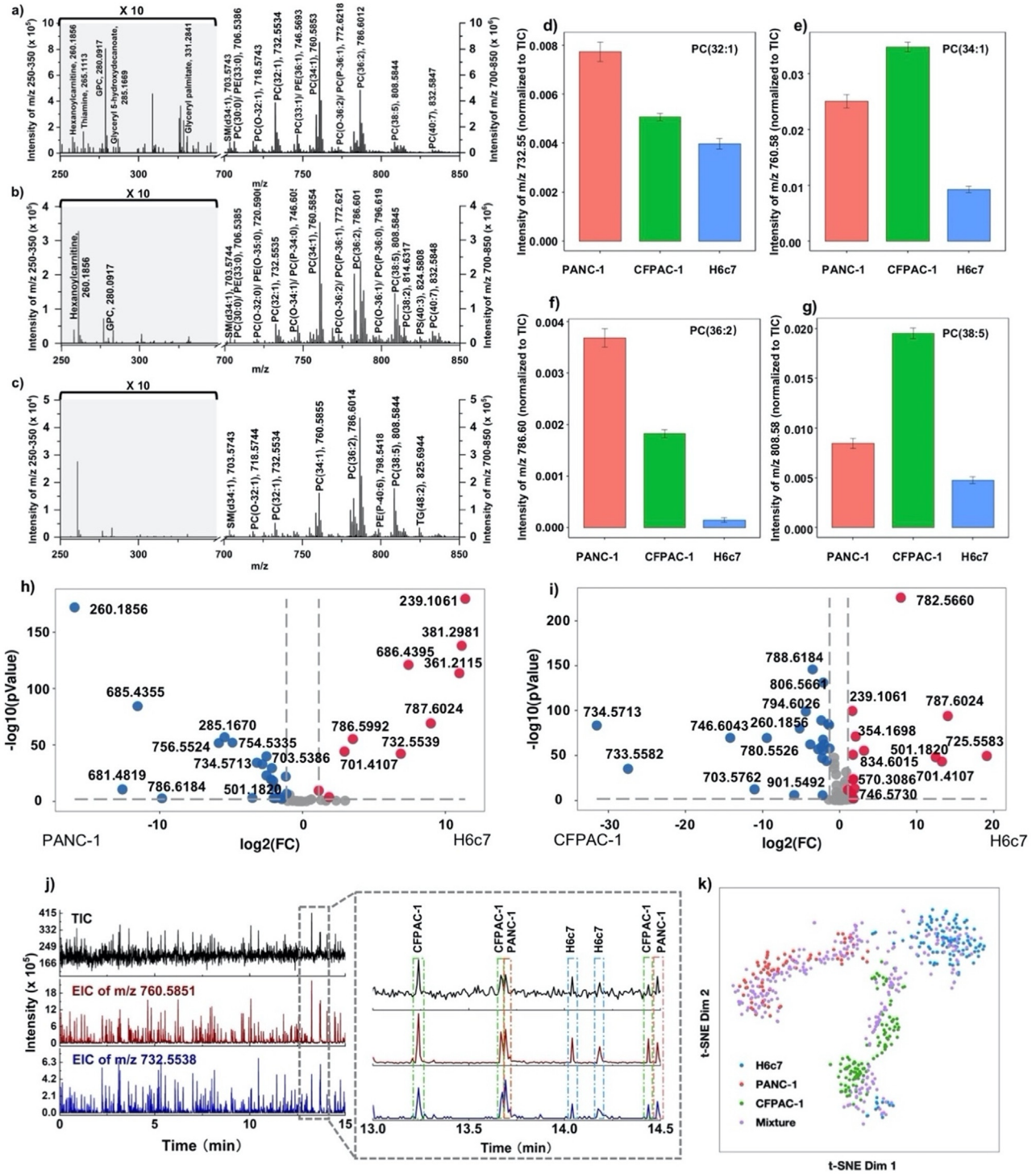

Figure 4. Assignment of cellular metabolites and discrimination of PDAC and H6c7 cells. a) Typical PANC-1 single-cell mass spectrum. b) Typical CFPAC-1 single-cell mass spectrum. c) Typical H6c7 single-cell mass spectrum. d–g) Normalized intensity of PC(32:1), PC(34:1), PC(36:2) and PC(38:5) in PANC-1, CFPAC-1 and H6c7 cells. h) Volcano plot of the correlations between the P-values and fold changes (FD) for the metabolite signals in PANC-1 and H6c7 cells. i) Volcano plot of the correlations between the P-values and fold changes (FD) for the metabolite signals in CFPAC-1 and H6c7 cells. j) Total ion chromatogram (TIC), extracted ion chromatogram (EIC) of *m/z* 760.5851 and EIC of *m/z* 732.5538 of mixed cell suspension (1×104 cells mL^{-1}) composed of PANC-1, CFPAC-1 and H6c7. k) Distributed stochastic neighbor embedding (t-SNE) analysis of PANC-1, CFPAC-1, H6c7 and mixed cell suspension composed of PANC-1, CFPAC-1 and H6c7.

conclude that the ACLY levels and lipid metabolism is deregulated in human PDAC. Recent studies revealed that PI3K-AKT and mTORC1 signaling pathways control the level of ACLY.[26,28] We thus hypothesized that the upregulated ACLY in PDAC cells may due to the deregulated PI3K-AKT and mTORC1 pathways. To this end, we monitored the

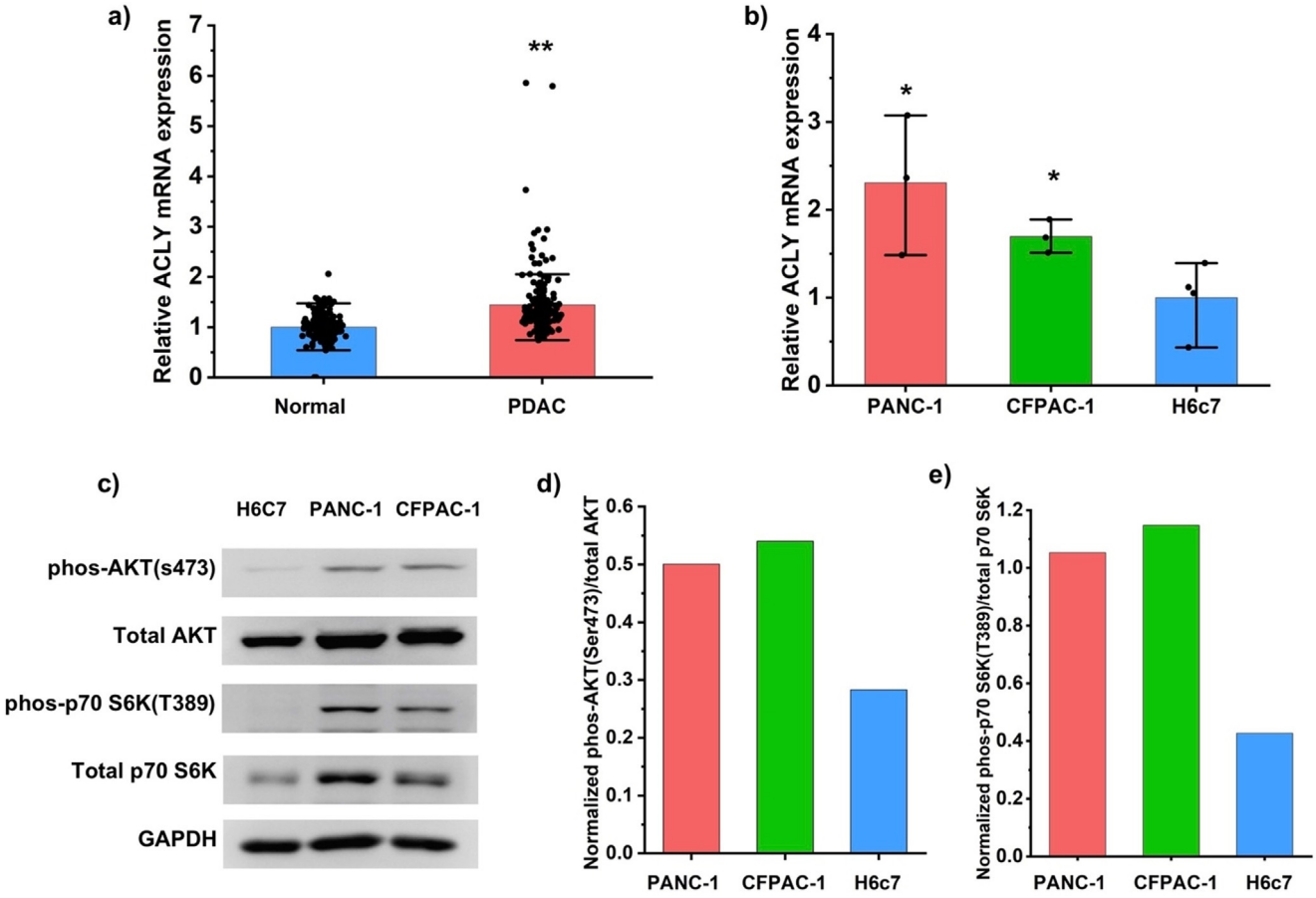

Figure 5. Deregulated ACLY levels in PDAC. a) Relative ACLY mRNA levels in human normal and PDAC pancreatic samples. Mean ± SD ($n=167$ in normal and $n=179$ in PDAC). **, $p<0.01$. b) Relative ACLY mRNA levels in PANC-1, CFPAC-1 and H6c7 cells. Mean ± SD ($n=3$). *, $p<0.05$. c) Immunoblot (IB) analysis of the total cell lysate derived from PANC-1, CFPAC-1 and H6c7 cells. GAPDH was used as protein loading control. d,e) Bar plots represent of the quantification of IB described in (c). qPCR and Immunoblot analysis were performed at the cell population level.

protein levels of the key members of both signalling pathways including: activated form of AKT (phosphorlation of AKT at ser473 site), total AKT, activated p70 S6K (phosphorlation of p70 S6K at T389 site) and total p70 S6K in PDAC and H6C7 cells by immunoblotting. Indeed, we found both signalling pathways are activated in PDAC cells evidenced by the upregulation of phos-AKT(Ser473)/total AKT and phos-p70 S6K(T389)/total p70 S6K levels compared to H6C7 cells (Figures 5c–e), indicating that the deregulated PI3K/AKT and mTORC1 pathways may contribute to the high levels of ACLY in PDAC cells.

ACLY Inhibition-Induced Lipid Redistribution Was Specifically Detected by the DBDI-MS Platform

Since the biological evidence demonstrates that ACLY is abundant in human PDAC samples, we investigated the effect of an ACLY chemical inhibitor on pancreatic cancer cells using the DBDI-MS platform. As shown in Figure 6a–g and S15a–g, PC(32:1), PC(34:1) and PC(36:2) are the three predominant lipids in PANC-1 and CFPAC-1. When PANC-1 and CFPAC-1 were treated with gemcitabine or DMSO, the intensity of PC(36:2) is higher than the intensity of PC(32:1), and the intensity ratio of PC(32:1)/PC(36:2) (m/z 732.55/786.60) is similar. However, when PANC-1 and CFPAC-1 were treated with SB-204990, the intensity of PC(36:2) became lower than intensity of PC(32:1), and the intensity ratio of PC(32:1)/PC(36:2) (m/z 732.55/786.60) was increased. Figure 6f and S15f show that compared with PANC-1 and CFPAC-1 cells treated with DMSO, the contents of PC(32:1), PC(34:1) and PC(36:2) in the cells treated with different concentrations of gemcitabine did not change significantly, but the contents of PC(32:1), PC(34:1) and PC(36:2) in PANC-1 and CFPAC-1 treated with different concentration of SB-204990 were significantly reduced, when the concentration of SB-204990 increased, the contents of PC(32:1), PC(34:1) and PC(36:2) decreased. The t-SNE clustering results in Figure 6h and S15h show heterogeneity of PANC-1 and CFPAC-1 after different treatments can be observed. PANC-1 and CFPAC-1 treated with SB-204990 were separated more significantly than PANC-1 and CFPAC-1 treated with gemcitabine or DMSO.

Thus, the above results show that the lipid metabolism in PDAC cells could be reversed by ACLY inhibition, which further supports the notion that deregulated ACLY contributes to the abundance of lipids in PDAC cells. Moreover, the modifications induced by ACLY inhibition could be specifi-

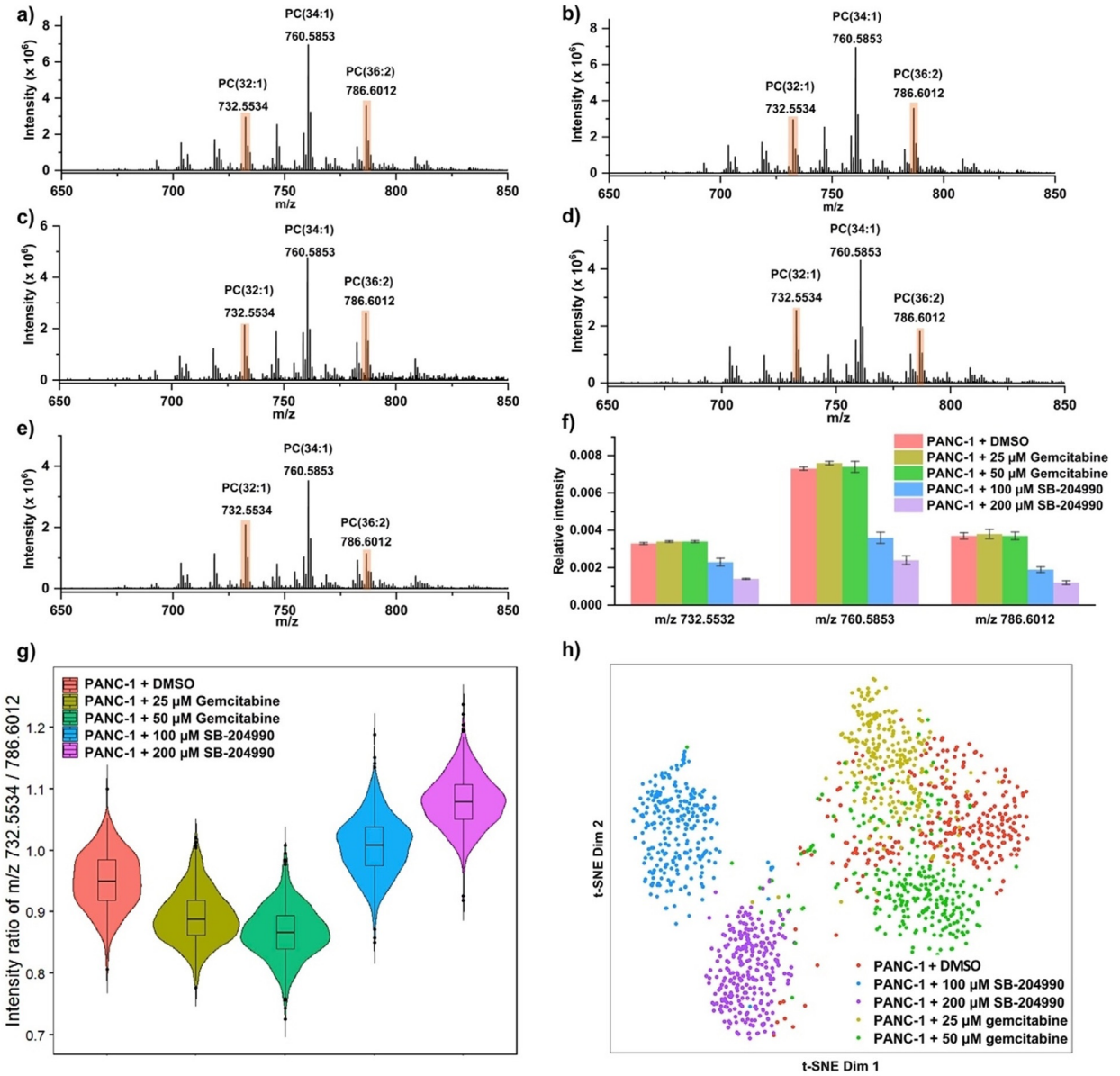

Figure 6. PANC-1 with different treatments. a) Representative mass spectrum of PANC-1 treated with DMSO. b) Representative mass spectrum of PANC-1 treated with 25 μM Gemcitabine. c) Representative mass spectrum of PANC-1 treated with 50 μM Gemcitabine. d) Representative mass spectrum of PANC-1 treated with 100 μM SB-204990. e) Representative mass spectrum of PANC-1 treated with 200 μM SB-204990. f) Bar plots for the changes of lipid contents after different treatments. g) Violin plots for comparing the intensity ratio of PC(32:1)/PC(36:2) (*m/z* 732.55/786.60) in PANC-1 with different treatments. h) t-SNE analysis of PANC-1 with different treatments.

cally detected by our sensitive single-cell DBDI-MS platform. Because DBDI-MS shows high sensitivity and high specificity at the level of cell lines, it has the potential to classify the cells in clinical cancer tissues, identify the characteristic metabolites of different cancer types, and distinguish cancer subtypes.

ACLY May Serve as a Novel Target for Established PDAC

The above findings revealed by our new DBDI platform inspired us to explore whether targeting ACLY could be beneficial for PDAC therapy. As a primitive ACLY inhibitor, SB-204990 displays tumor-suppressive effects in multiple tumors both in vitro and in vivo.[29]

To this end, we first treated PANC-1 and CFPAC-1 cells with the ACLY inhibitor SB-204990 and found a dosage dependent suppression of cell viability by SB-204990 in PDAC cells (Figures 7a and d). Accordingly, after transfecting PDAC cells with siRNA targeting ACLY (Figures 7b and e), we also found a significant reduction of cell viability (Figures 7c and f). Thus both chemical inhibitors or genetic approaches targeting ACLY could reduce PDAC cell viability, suggesting that ACLY could be a promising target in established PDAC.

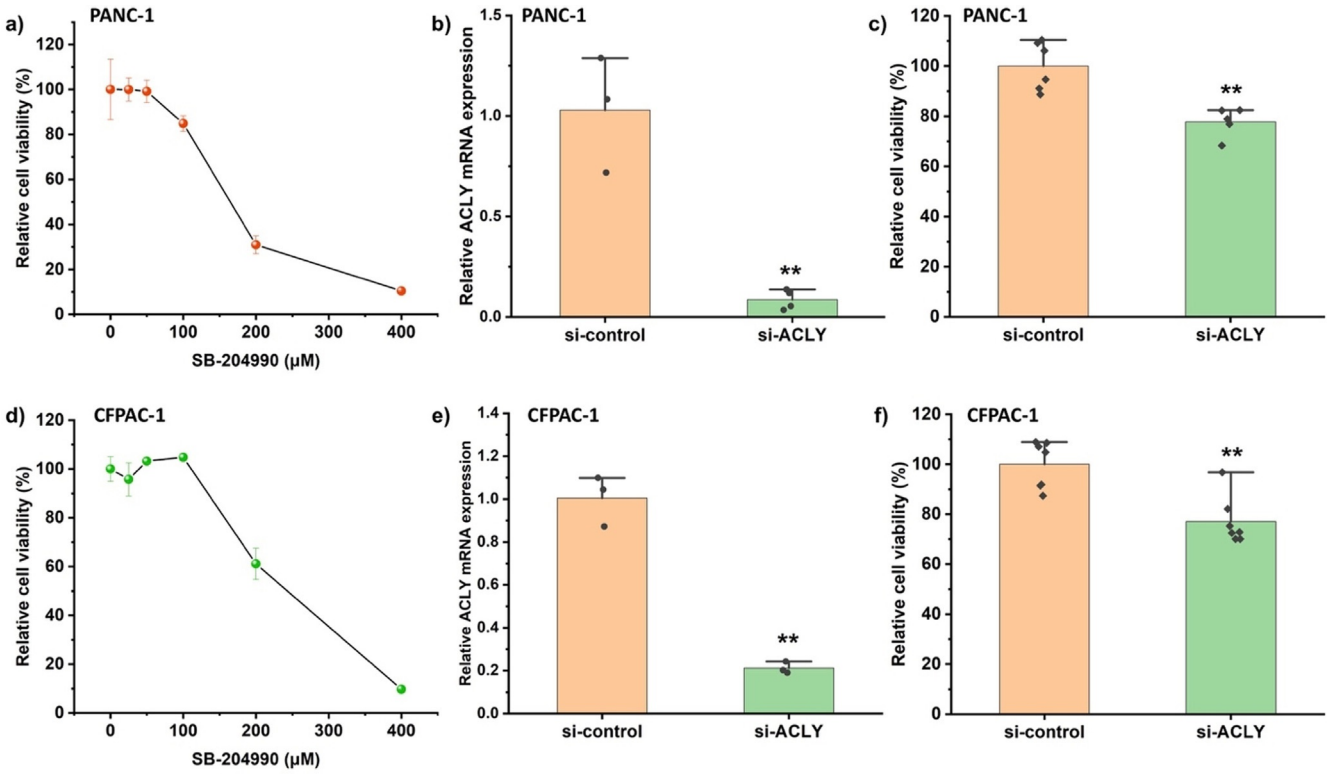

Figure 7. Chemical inhibition or siRNA approach targeting ACLY suppress PDAC cell viability at the population level. a,d) Relative cell viability detected by MTT assay in PANC-1 and CFPAC-1 cells treated with indicated concentration of SB-204990 and DMSO for 48 hours. Mean ± SD ($n = 4$–8). b,e) Relative ACLY mRNA expression in PANC-1 and CFPAC-1 cells transfected with si-control or si-*Acly* oligos. Mean ± SD ($n = 3$–4). **, $p < 0.01$, unpaired *t*-test. e,f) Relative cell viability detected by MTT assay in PANC-1 and CFPAC-1 cells transfected with si-control or si-*Acly* oligos for 72 hours. Mean ± SD ($n = 6$). **, $p < 0.01$, unpaired *t*-test.

Conclusion

In conclusion, a high-throughput, label-free and sensitive DBDI-MS platform was developed for the analysis of single-cell metabolites, which achieved a throughput of approximately 38 cells per minute. The DBDI-MS platform is able to discriminate different cell types successfully based on their cellular metabolites. Compared with bulk cell analysis, our single-cell DBDI-MS platform can separate different cells from mixed cell suspensions according to its characteristic single-cell metabolite profile, and classify each type of cell into a specific group, which may help detect lipid metabolism in clinical cancer tissues.

Since the DBDI-MS platform found that abnormal lipid metabolism occurs in pancreatic cancer cells, a series of biological methods were used to analyze the expression levels of ACLY and the activation of related biological pathways in the TCGA dataset and PDAC cells. We indeed found the deregulated ACLY, acetyl-CoA synthesis and lipid homeostasis pathways in PDAC. We further identified deregulated PI3K/AKT and mTORC1 pathways may promote the ACLY expression in PDAC.

By treating PDAC cells with different dosages of specific ACLY inhibitor, the redistribution of lipids in PDAC cells was observed by the DBDI-MS platform. Further biological experiments also demonstrated that both ACLY inhibitor or genetic approach that targeting ACLY could repress cell viability of PDAC cells. These results prove the high sensitivity of our DBDI-MS platform and also confirmed that ACLY indeed contributes to the lipid metabolism in PDAC cells, indicating ACLY may serve as a novel therapeutic target in PDAC.

Thus, our DBDI-MS platform may have the potential to serve as a new generation of mass cytometry and contribute to biological and clinical research.

Acknowledgements

Q. Liu thanks the China Scholarship Council (CSC) for financial support of her Ph.D. research (Grant Number: 201906240053). We thank all members of the Zenobi group, especially Dr. Ri Wu and Alina Begley for helpful discussion and suggestions. We thank Marco Zesiger and Christian Marro from the ETH mechanical workshop for the fabrication of the cell introduction system, active capillary plasma source and other relevant parts. We thank Yuliang He for the bioinformatic analysis (Figure S14). Table of Contents, Figure 1 and Figure S1 were created with BioRender.com. The original data used in this publication have been made available in a curated data archive at ETH Zurich (https://www.researchcollection.ethz.ch) under the https://doi.org/10.3929/ethz-b-000484238. Open access funding provided by Eidgenossische Technische Hochschule Zurich.

Conflict of Interest

The authors declare no conflict of interest.

Keywords: ATP citrate lyase · dielectric barrier discharge · ionization sources · lipid metabolism · single-cell mass spectrometry

[1] M. Ackermann, *Nat. Rev. Microbiol.* **2015**, *13*, 497 – 508.
[2] R. Zenobi, *Science* **2013**, *342*, 1243259.
[3] a) A. Jindal, P. Gupta, Jayadeva, D. Sengupta, *Nat. Commun.* **2018**, *9*, 4719; b) C. Alix-Panabières, K. Pantel, *Cancer Discovery* **2016**, *6*, 479.
[4] a) D. A. Lawson, N. R. Bhakta, K. Kessenbrock, K. D. Prummel, Y. Yu, K. Takai, A. Zhou, H. Eyob, S. Balakrishnan, C. Y. Wang, P. Yaswen, A. Goga, Z. Werb, *Nature* **2015**, *526*, 131 – 135; b) J. R. Heath, A. Ribas, P. S. Mischel, *Nat. Rev. Drug Discovery* **2016**, *15*, 204 – 216; c) T. Stuart, R. Satija, *Nat. Rev. Genet.* **2019**, *20*, 257 – 272.
[5] R. T. Davis, K. Blake, D. Ma, M. B. I. Gabra, G. A. Hernandez, A. T. Phung, Y. Yang, D. Maurer, A. E. Y. T. Lefebvre, H. Alshetaiwi, Z. Xiao, J. Liu, J. W. Locasale, M. A. Digman, E. Mjolsness, M. Kong, Z. Werb, D. A. Lawson, *Nat. Cell Biol.* **2020**, *22*, 310 – 320.
[6] D. Hanahan, R. A. Weinberg, *Cell* **2011**, *144*, 646 – 674.
[7] N. N. Pavlova, C. B. Thompson, *Cell Metab.* **2016**, *23*, 27 – 47.
[8] P. Rawla, T. Sunkara, V. Gaduputi, *World J. Oncol.* **2019**, *10*, 10 – 27.
[9] H. Chang, A. Moro, K. Takakura, H. Su, A. Mo, M. Nakanishi, R. T. Waldron, S. W. French, D. W. Dawson, O. J. Hines, G. Li, V. L. W. Go, J. Sinnett-Smith, S. J. Pandol, A. Lugea, A. S. Gukovskaya, M. O. Duff, D. W. Rosenberg, E. Rozengurt, G. Eibl, *PLoS ONE* **2017**, *12*, e0184455.
[10] J. Fan, K. Slowikowski, F. Zhang, *Exp. Mol. Med.* **2020**, *52*, 1452 – 1465.
[11] M. L. Suvà, I. Tirosh, *Mol. Cell* **2019**, *75*, 7 – 12.
[12] a) T. D. Do, T. J. Comi, S. J. Dunham, S. S. Rubakhin, J. V. Sweedler, *Anal. Chem.* **2017**, *89*, 3078 – 3086; b) H. Lim, S. Y. Lee, Y. Park, H. Jin, D. Seo, Y. H. Jang, D. W. Moon, *Nat. Methods* **2021**, *18*, 316 – 320; c) H. Tian, L. J. Sparvero, P. Blenkinsopp, A. A. Amoscato, S. C. Watkins, H. Bayir, V. E. Kagan, N. Winograd, *Angew. Chem. Int. Ed.* **2019**, *58*, 3156 – 3161; *Angew. Chem.* **2019**, *131*, 3188 – 3193.
[13] a) A. Amantonico, J. Y. Oh, J. Sobek, M. Heinemann, R. Zenobi, *Angew. Chem. Int. Ed.* **2008**, *47*, 5382 – 5385; *Angew. Chem.* **2008**, *120*, 5462 – 5465; b) M. Kompauer, S. Heiles, B. Spengler, *Nat. Methods* **2017**, *14*, 90 – 96; c) E. K. Neumann, T. J. Comi, S. S. Rubakhin, J. V. Sweedler, *Angew. Chem. Int. Ed.* **2019**, *58*, 5910 – 5914; *Angew. Chem.* **2019**, *131*, 5971 – 5975.
[14] a) T. Fujii, S. Matsuda, M. L. Tejedor, T. Esaki, I. Sakane, H. Mizuno, N. Tsuyama, T. Masujima, *Nat. Protoc.* **2015**, *10*, 1445 – 1456; b) R. M. Onjiko, S. A. Moody, P. Nemes, *Proc. Natl. Acad. Sci. USA* **2015**, *112*, 6545 – 6550; c) N. Pan, S. J. Standke, N. R. Kothapalli, M. Sun, R. C. Bensen, A. W. G. Burgett, Z. Yang, *Anal. Chem.* **2019**, *91*, 9018 – 9024.
[15] S. A. Stopka, R. Khattar, B. J. Agtuca, C. R. Anderton, L. Pasa-Tolic, G. Stacey, A. Vertes, *Front. Plant Sci.* **2018**, *9*, 1646.
[16] R. Liu, N. Pan, Y. Zhu, Z. Yang, *Anal. Chem.* **2018**, *90*, 11078 – 11085.
[17] a) C. Lombard-Banek, S. A. Moody, P. Nemes, *Angew. Chem. Int. Ed.* **2016**, *55*, 2454 – 2458; *Angew. Chem.* **2016**, *128*, 2500 – 2504; b) C. Lombard-Banek, S. A. Moody, M. C. Manzini, P. Nemes, *Anal. Chem.* **2019**, *91*, 4797 – 4805; c) C. Lombard-Banek, J. Li, E. P. Portero, R. M. Onjiko, C. D. Singer, D. O. Plotnick, R. Q. Al Shabeeb, P. Nemes, *Angew. Chem. Int. Ed.* **2021**, *60*, 12852 – 12858; *Angew. Chem.* **2021**, *133*, 12962 – 12968.
[18] a) H. W. Jackson, J. R. Fischer, V. R. T. Zanotelli, H. R. Ali, R. Mechera, S. D. Soysal, H. Moch, S. Muenst, Z. Varga, W. P. Weber, B. Bodenmiller, *Nature* **2020**, *578*, 615 – 620; b) J. Wagner, M. A. Rapsomaniki, S. Chevrier, T. Anzeneder, C. Langwieder, A. Dykgers, M. Rees, A. Ramaswamy, S. Muenst, S. D. Soysal, A. Jacobs, J. Windhager, K. Silina, M. van den Broek, K. J. Dedes, M. Rodriguez Martinez, W. P. Weber, B. Bodenmiller, *Cell* **2019**, *177*, 1330 – 1345.
[19] a) S. Xu, M. Liu, Y. Bai, H. Liu, *Angew. Chem. Int. Ed.* **2021**, *60*, 1806 – 1812; *Angew. Chem.* **2021**, *133*, 1834 – 1840; b) H. Yao, H. Zhao, X. Zhao, X. Pan, J. Feng, F. Xu, S. Zhang, X. Zhang, *Anal. Chem.* **2019**, *91*, 9777 – 9783.
[20] a) A. Albert, C. Engelhard, *Anal. Chem.* **2012**, *84*, 10657 – 10664; b) L. Bregy, P. M. Sinues, M. M. Nudnova, R. Zenobi, *J. Breath Res.* **2014**, *8*, 027102; c) J. I. Zhang, W. A. Tao, R. G. Cooks, *Anal. Chem.* **2011**, *83*, 4738 – 4744.
[21] a) B. Gilbert-López, H. Geltenpoth, C. Meyer, A. Michels, H. Hayen, A. Molina-Diaz, J. F. Garcia-Reyes, J. Franzke, *Rapid Commun. Mass Spectrom.* **2013**, *27*, 419 – 429; b) F. J. Lara-Ortega, J. Robles-Molina, S. Brandt, A. Schutz, B. Gilbert-Lopez, A. Molina-Diaz, J. F. Garcia-Reyes, J. Franzke, *Anal. Chim. Acta* **2018**, *1020*, 76 – 85.
[22] A. K. Huba, M. F. Mirabelli, R. Zenobi, *Anal. Chim. Acta* **2018**, *1030*, 125 – 132.
[23] Q. Liu, R. Zenobi, manuscript in preparation.
[24] Q. Liu, R. Zenobi, *Rapid Commun. Mass Spectrom.* **2020**, *34*, e9021.
[25] J. Swierczynski, A. Hebanowska, T. Sledzinski, *World J. Gastroenterol.* **2014**, *20*, 2279 – 2303.
[26] A. Carrer, S. Trefely, S. Zhao, S. L. Campbell, R. J. Norgard, K. C. Schultz, S. Sidoli, J. L. D. Parris, H. C. Affronti, S. Sivanand, S. Egolf, Y. Sela, M. Trizzino, A. Gardini, B. A. Garcia, N. W. Snyder, B. Z. Stanger, K. E. Wellen, *Cancer Discovery* **2019**, *9*, 416.
[27] B. J. Raphael, R. H. Hruban, A. J. Aguirre, et al., *Cancer Cell* **2017**, *32*, 185 – 203.
[28] A. J. Covarrubias, H. I. Aksoylar, J. Yu, N. W. Snyder, A. J. Worth, S. S. Iyer, J. Wang, I. Ben-Sahra, V. Byles, T. Polynne-Stapornkul, E. C. Espinosa, D. Lamming, B. D. Manning, Y. Zhang, I. A. Blair, T. Horng, *eLife* **2016**, *5*, e11612.
[29] G. Hatzivassiliou, F. Zhao, D. E. Bauer, C. Andreadis, A. N. Shaw, D. Dhanak, S. R. Hingorani, D. A. Tuveson, C. B. Thompson, *Cancer Cell* **2005**, *8*, 311 – 321.

Manuscript received: May 30, 2021
Revised manuscript received: August 17, 2021
Accepted manuscript online: September 10, 2021
Version of record online: October 11, 2021

